Journal of Geodesy (2005)
DOI 10.1007/s00190-004-0417-y

Journal of Geodesy

Interannual variability of low-degree gravitational change, 1980–2002

J.L. Chen[1], C.R. Wilson[1,2], B.D. Tapley[1]

[1] Center for Space Research, University of Texas, Austin, TX 78712, USA;
e-mail: chen@csr.utexas.edu; Tel.: 512-232-6218; Fax: 512-471-3570
[2] Department of Geological Sciences, University of Texas, Austin, TX 78712, USA

Received: 22 March 2004 / Accepted: 4 October 2004 / Published online: 21 March 2005

Abstract. Time variations in the Earth's gravity field at periods longer than 1 year, for degree-two spherical harmonics, ΔC_{21}, ΔS_{21}, and ΔC_{20}, are estimated from accurately measured Earth rotational variations. These are compared with predictions of atmospheric, oceanic, and hydrologic models, and with independent satellite laser ranging (SLR) results. There is remarkably good agreement between Earth rotation and model predictions of ΔC_{21} and ΔS_{21} over a 22-year period. After decadal signals are removed, Earth-rotation-derived interannual ΔC_{20} variations are dominated by a strong oscillation of period about 5.6 years, probably due to uncertainties in wind and ocean current estimates. The model-predicted ΔC_{20} agrees reasonably well with SLR observations during the 22-year period, with the exception of the recent anomaly since 1997/1998.

Key words: Interannual gravity change – Earth rotation – Low-degree harmonics

1 Introduction

Mass redistribution and transport within the Earth system introduce changes in the Earth's rotation and gravity field as observed by space geodetic techniques, including very long baseline interferometry (VLBI), the global positioning system (GPS), and satellite laser ranging (SLR). These highly precise space geodetic observations provide indirect global measures of mass redistribution within the Earth system. There are important contributions from air and water redistribution associated with weather and climate, but contributions also come from the mantle and core (see e.g. Chao and Gross 1987; Hide at al. 1993).

Correspondence to: J.L. Chen

Time variations in the degree-two zonal term of the Earth's gravity field (i.e. ΔC_{20}) are believed to be well determined from SLR, and show variability over a broad range of periods (see e.g. Yoder et al. 1983; Cheng et al. 1997; Pavlis 2001; Cox and Chao 2002). At seasonal and shorter time scales, SLR determinations of ΔC_{20} agree fairly well with atmospheric, oceanic, and hydrological model predictions (see e.g. Chao and Eanes 1995; Chen et al. 1999). A long-term increase in ΔC_{20} is related to redistribution of water mass at the end of the last ice age, as rebound of the ice-deformed crust and mantle continues to the present day (see e.g. Yoder et al. 1983; Rubincam 1984).

Cox and Chao (2002) discovered a ΔC_{20} anomaly beginning in 1998, roughly coincident with the 1997/1998 E1 Niño event, but persisting beyond the generally recognized E1 Niño period. This inspired several studies seeking a physical explanation for the anomaly (see e.g. Dickey et al. 2002; Nerem et al. 2002; Chao et al. 2003; Chen et al. 2003). Large-scale mass redistribution within the Earth system starting around 1998 is the accepted mechanism, but available atmospheric, oceanic, and hydrologic models do not yet provide a full explanation.

The Earth's rotational changes at periods of several years and less are forced mainly by surface mass redistribution within the Earth system (see e.g. Barnes et al. 1983; Chao and Au 1991; Dickey et al. 1993; Ponte et al. 1998; Chen et al. 2000). Changes in Earth orientation parameters (EOPs) including polar motion (X_p, Y_p) and length of day (LOD) due to surface mass load variations are proportional to changes in degree-two harmonic (Stokes) coefficients, ΔC_{21}, ΔS_{21}, and ΔC_{20} (see e.g. Chao 1994; Eubanks 1993; Chen et al. 2000; Chen and Wilson 2003; Marchenko and Schwintzer 2003; Gross et al. 2004a). Thus, EOP time series provide an independent estimate of time variations in these components of the Earth's gravity field if wind and ocean current effects, estimated from atmospheric and ocean models, are subtracted. It is also necessary to assume that the influence of other elements of the Earth system (mantle and core) can be separated on the basis of the time scale of variations.

Previous studies (Chen et al. 2000; Chen and Wilson 2003) demonstrated that EOPs provide a better determination of ΔC_{21} and ΔS_{21} than SLR data at seasonal and shorter time scales. However, SLR estimates of ΔC_{20} are apparently superior to EOP results, because there is better agreement with geophysical model predictions (see e.g. Chao and Eanes 1995; Chen et al. 1999; Cheng and Tapley 1999). A recent study by Gross et al. (2004a) concludes that EOP-derived ΔC_{21}, ΔS_{21}, and ΔC_{20} also agree reasonably well with GPS estimates. EOP determinations of ΔC_{20} are more difficult because winds are the dominant excitation source. Thus, small errors in removing the wind contribution produce large errors in estimates of ΔC_{20}.

Most previous studies (see e.g. Chao and O'Connor 1988; Chao and Eanes 1995; Chen et al. 1999; Cheng and Tapley 1999, Nerem et al. 2000) have compared geophysical model predictions with gravity changes at periods of a year and less, but here we examine longer-period variations. Starting with EOP time series, we subtract wind and current effects, and compare estimated gravity changes with predictions from atmospheric, oceanic, and hydrologic models. The main objectives are to examine the feasibility of using EOP series to estimate longer period variations of ΔC_{21}, ΔS_{21}, and ΔC_{20}, and to examine related properties of numerical climate models at these periods.

2 Theory

2.1 Gravitational change

The geopotential field is conveniently expressed in a spherical harmonic expansion as (see e.g. Lambeck 1980; Chao 1994)

$$U(r,\theta,\lambda) = \frac{GM}{r}\left[1 + \sum_{l=2}^{\infty}\sum_{m=0}^{l}\left(\tfrac{R}{r}\right)^l \bar{P}_{lm}(\cos\theta) \times (C_{lm}\cos m\lambda + S_{lm}\sin m\lambda)\right] \quad (1)$$

where r is radius, θ co-latitude, and λ longitude. R is the Earth's mean radius on the surface, M the Earth's mass, G the gravitational constant; $\bar{P}_{lm}$ is the 4π-normalized associated Legendre function of degree l and order m (equal to $[(2-\delta_{m0})(2l+1)(l-m)!/(l+m)!]^{1/2}$ times the ordinary associated Legendre function) (Chao 1994), and C_{lm} and S_{lm} are the normalized harmonic or Stokes coefficients. Changes in C_{lm} and S_{lm} are related to changes in the Earth's density distribution $\Delta\rho(r,\theta,\lambda)$ via (Chao and Gross 1987; Chao 1994)

$$\begin{Bmatrix}\Delta C_{lm}\\ \Delta S_{lm}\end{Bmatrix} = \frac{1}{(2l+1)M}\int \Delta\rho(r,\theta,\lambda)\left(\tfrac{r}{R}\right)^l \bar{P}_{lm} \times (\cos\theta)\begin{Bmatrix}\cos m\lambda\\ \sin m\lambda\end{Bmatrix} \mathrm{d}V \quad (2)$$

For surface mass variations, e.g. changes in atmospheric surface pressure, ocean bottom pressure, and continental water storage change, Eq. (2) can be simplified to a surface integral with element $\mathrm{d}s = R^2\sin\theta\ \mathrm{d}\theta\ \mathrm{d}\lambda$

$$\begin{Bmatrix}\Delta C_{lm}\\ \Delta S_{lm}\end{Bmatrix} = \frac{(1+k'_l)}{(2l+1)M}\int \Delta\sigma(\theta,\lambda)\bar{P}_{lm} \times (\cos\theta)\begin{Bmatrix}\cos m\lambda\\ \sin m\lambda\end{Bmatrix}\mathrm{d}s \quad (3)$$

The above equation takes into explicit consideration the yielding effect of the solid Earth in terms of the so-called load Love number k'_l, whose values are estimated for the Earth based on an idealized Earth model (Farrel 1972), for example $k'_2 = -0.301$, $k'_3 = -0.20$, etc. $\Delta\sigma$ represents surface density change (or mass load change).

The degree 2 order 0 and 1 ordinary associated Legendre functions can be expressed as [Eubanks 1993, Eq. (A2-2a)]

$$P_{2,0} = (3\sin^2(\theta) - 1)/2$$
$$P_{2,1} = 3\cos\theta\sin\theta \quad (4)$$

and accordingly the normalized associated Legendre functions can be computed by applying the normalization factor given above [below Eq. (1)] to Eq. (4) as

$$\bar{P}_{2,0} = \sqrt{5}\cdot(3\sin^2(\theta) - 1)/2$$
$$\bar{P}_{2,1} = \sqrt{\tfrac{5}{3}}\cdot 3\cos\theta\sin\theta \quad (5)$$

2.2 Interpreting EOPs in terms of Stokes's coefficient change

The effective Earth rotational excitations (χ_1, χ_2, χ_3) caused by surface mass load change can be computed via [Eubanks 1993, Eqs. (A3-1), (A3-3)]

$$\chi_1 = -\frac{1.098R^2}{(C-A)}\iint \Delta\sigma(\theta,\lambda,t)\sin(\theta)\cos(\theta)\cos\lambda\ \mathrm{d}s$$
$$\chi_2 = -\frac{1.098R^2}{(C-A)}\iint \Delta\sigma(\theta,\lambda,t)\sin(\theta)\cos(\theta)\sin\lambda\ \mathrm{d}s$$
$$\chi_3 = \frac{0.753R^2}{C_m}\iint \Delta\sigma(\theta,\lambda,t)\cos(\theta)^2\mathrm{d}s \quad (6)$$

where C (8.0376×10^{37} kg m^2) and A (C–A $= 2.61\times10^{35}$ kg m^2) are the two principal inertia moments of the Earth, and C_m (7.1236×10^{37} kg m^2) is the principal inertia moments of the Earth's mantle (Eubanks 1993). The use of numerical values from Eubanks (1993) is for consistency with our earlier results (Chen et al. 2000; Chen and Wilson 2003). We realize that the numerical values have been updated (see e.g. the IERS2003 Convention), which may introduce slight change in the estimates.

Combining Eqs. (3), (5), and (6) gives the relationship between mass load-induced Earth rotational excitations (χ_1, χ_2, χ_3) and the degree-two Stokes coefficient changes (ΔC_{21}, ΔS_{21}, ΔC_{20}) [Chao 1994, Eqs. (5), and (14); Chen and Wilson 2003, Eq. (1)] as

$$\Delta C_{21} = -(1+k_2') \cdot \sqrt{\frac{3}{5}} \cdot \frac{(C-A)}{1.098R^2M} \cdot \chi_1$$
$$\Delta S_{21} = -(1+k_2') \cdot \sqrt{\frac{3}{5}} \cdot \frac{(C-A)}{1.098R^2M} \cdot \chi_2 \quad (7)$$

and

$$\Delta C_{20} = -(1+k_2') \times \left[\frac{3}{2\sqrt{5}} \cdot \frac{C_m}{0.753R^2M} \cdot \chi_3 + \frac{1}{2\sqrt{5}} \cdot \frac{\Delta T}{MR^2}\right] \quad (8)$$

where ΔT is a change in the trace of the Earth's inertia tensor, the sum of its moments of inertia [Rochester and Smylie 1974, Eq. (1)]. $\Delta T/2R^2$ represents the total mass change on a sphere's surface (when only considering surface mass loads). $\Delta C_{20} = -\Delta J_2/\sqrt{5}$ (as ΔJ_2 is used in some of the cited articles). As demonstrated through the step-by-step derivation from the above [Eqs. (1)–(8), the factor $(1+k_2')$ is necessary and represents the elastic yielding effects. Equations (7) and (8) are the fully normalized version of Eq. (1) in Chen et al. (2000), which represents the un-normalized change in ΔC_{21}, ΔS_{21}, and ΔC_{20}.

After computing the excitation function time series from observed polar motion (Wilson 1985), and subtracting wind and ocean current effects, we convert the residual time series (χ_1, χ_2) to fully normalized ΔC_{21} and ΔS_{21} using Eq. (7). Rotational deformation effects on observed excitations are modeled and removed through effective wind and ocean current excitations via the numerical factors [Eubanks 1993, Eq. (A3-2), (A3-4)]. Therefore, ΔC_{21} and ΔS_{21} estimated from Eq. (7) represent gravitational change associated with mass load change only. Similarly, after wind and ocean current effects are subtracted from observed LOD excitations ($\chi_3 = \Delta\text{LOD/LOD}$), residual changes in observed χ_3 are used to compute the fully normalized Stokes coefficient ΔC_{20} via Eq. (8). As Rochester and Smylie (1974) show, it is reasonable to take ΔT to be exactly zero when considering deformation of the Earth but, in the present case, redistribution of air and water changes mass elevation, hence moment of inertia. We calculated a time series of ΔT using atmospheric pressure and terrestrial water storage loads from the models, and found typical annual ΔC_{20} variability due to ΔT change to be about 1×10^{-13}, less than 0.1% of the variations measured by SLR. At longer periods, where postglacial rebound is dominant, a ΔT contribution from melting mountain glaciers is probably below the 1% level. Therefore, we neglect ΔT effects in our analysis.

3 Data and data processing

3.1 Earth rotation and SLR observations

Polar motion (X_p,Y_p) and LOD time series are taken from the SPACE 2002 data set (Gross 2002). Daily values are determined from various space geodetic observations by a Kalman filter combination. Time series cover the period September 1976 through to January 2003. The effects of the long-period solid Earth and ocean tides on the observed LOD changes are removed using the models of Yoder et al. (1981) and Kantha et al. (1998), respectively. Excitation functions are computed from (X_p,Y_p) using the discrete linear polar motion filter developed by Wilson (1985), using a Chandler frequency of 0.843 cycles per year (CPY) and a quality factor (Q) of 175.

SLR estimates of ΔC_{20} are provided by C. Cox (pers. Commun 2003), and are identical to published values (Cox and Chao 2002), with an additional year of data obtained since that publication. The first-order data processing step is to remove a linear trend, assumed due to postglacial rebound, to leave residual interannual, seasonal, and shorter-period fluctuations. We subtract the estimated rate of change of ΔC_{20}, 1.25×10^{-11} per year [corresponding to a ΔJ_2 rate of $-2.8 \times 10^{-11} \pm 0.4$ per year (Cox and Chao 2002)]. Seasonal or shorter period variations are removed by a 1-year sliding window filter.

Independent information about long-term changes in ΔC_{20} comes from observed eclipses in the historical record extending to 2700 years before present. Stephenson and Morrison (1995) estimate the non-tidal rate of change of LOD to be $(-0.6 \pm 0.1) \times 10^{-5}$ s per year based on historical eclipse data. In the absence of external torques (e.g. wind and current frictions), the product of moment of inertia C and angular velocity Ω remains constant, implying that the rate of change of moment of inertia is $\Delta C = C^*\Delta\text{LOD/LOD}$. Because long-term changes in the trace of the inertia tensor are probably small, as discussed below, ΔC is directly proportional to the rate of change of ΔC_{20}. Therefore, the eclipse data provide an estimated rate of change of ΔC_{20} equal to $-1.55 (\pm 0.27) \times 10^{-11}$ per year. This assumes that the mantle and core are fully coupled, so that C is mantle plus core moment of inertia. The Stephenson–Morrison rate is consistent with SLR results, though not strongly. If the core and mantle are not coupled, the mantle moment of inertia is used instead, reducing the Stephenson–Morrison estimate to 1.38×10^{-11} per year, more concordant with the SLR results. Thus, SLR and eclipse data, taken together, might suggest that complete coupling of mantle and core occurs at time scales exceeding the 2700-year period measured by the eclipse data. Countering this suggestion is the possibility that the SLR rate for ΔC_{20} is contaminated by decadal-scale variations of shorter-term climatic origin. This is a reasonable possibility, following the discovery by Cox and Chao (2002) of a ΔC_{20} anomaly lasting several years.

3.2 Oceanic model

We use the ECCO Ocean General Circulation Model (OGCM), based on the parallel version of the Massachusetts Institute of Technology general circulation model (Fukumori et al. 2000). ECCO coverage is nearly global from 72.5°S to 72.5°N and has a telescoping meridional grid with 1/3-degree resolution in the tropics (20°S to 20°N) that gradually increases to 1-degree

resolution away from the equator. The resolution in longitude is 1 degree. There are 46 vertical levels with 10-m resolution within 150 m of the surface. ECCO is forced by the National Center for Environmental Prediction (NCEP) reanalysis products (12-hourly wind stress, daily heat and fresh water fluxes) with time means replaced by those of the Comprehensive Ocean–Atmosphere Data Set. Surface temperature and salinity are relaxed towards observed values. ECCO fields are available as 10-day averages. Sea surface height and ocean bottom pressure (OBP) are also available at 12-hour intervals, as instantaneous values. These OBP data are used to estimate oceanic contributions to ΔC_{21}, ΔS_{21}, and ΔC_{20} time series using Eq. (3), and are then averaged and re-sampled to monthly average values. Ocean current effects on observed X_p, Y_p, and LOD excitations are removed using the ocean current component of the ocean angular momentum (OAM) products computed from the same ECCO model by Gross et al. (2003).

3.3 Hydrologic Model

Continental water storage fields are taken from the Land Data Assimilation System (LDAS), a surface hydrologic model recently developed at the NCEP Climate Prediction Center (CPC) (Fan et al. 2003). LDAS is forced by observed precipitation, derived from CPC daily and hourly precipitation analyses, downward solar and longwave radiation, surface pressure, humidity, 2-m temperature and horizontal wind speed from NCEP reanalysis. The output consists of soil temperature and soil moisture in four layers below the ground. At the surface, it includes all components affecting energy and water mass balance, including snow cover, depth, and albedo. The model provides the information needed to route runoff into stream flow, allowing a calculation of river and stream angular momentum fluctuations. Monthly average soil water storage changes are provided on a $0.5^\circ \times 0.5^\circ$ grid for the period January 1980 to July 2003. We use these monthly fields to estimate contributions to ΔC_{21}, ΔS_{21}, and ΔC_{20} using Eq. (3).

3.4 Atmospheric model and mass conservation

Surface atmospheric pressure from the NCEP reanalysis is used to compute atmospheric contributions to ΔC_{21}, ΔS_{21}, and ΔC_{20} via Eq. (3). Daily averages are available for the period January 1948 to present, on a Gaussian grid, about 1.904° latitude by 1.875° longitude, and are averaged to form monthly samples. An inverted barometer (IB) correction is applied so that, over the oceans, atmospheric pressure at any point is replaced by mean pressure over the oceans. Wind contributions are computed from NCEP reanalysis atmospheric angular momentum (AAM) products (Salstein and Rosen 1997).

Mass conservation is introduced when forming the sum of atmospheric, oceanic, and hydrologic effects. The first step is to constrain the ECCO OBP fields to conserve total ocean mass. Then a uniform layer of water is added to the oceans, equal to the total water mass change over land. Finally, the change of the total mass of the atmosphere is balanced by adding a uniform layer of water to the oceans and land. The application of mass conservation in the Earth system only has minor effects on the degree-two Stokes coefficients computation. However, it does have relatively larger effects on the degree-one coefficients, i.e. the geocenter motion (Chen et al. 1999), and significantly affects the degree-zero coefficient computation (Gross et al. 2004b).

4 Results

Figure 1a,b,c show ΔC_{21}, ΔS_{21}, and ΔC_{20} estimates from χ_1, χ_2, and χ_3, after removing wind and current contributions. These are compared with mass-redistribution estimates from geophysical models, i.e. the combined oceanic, hydrologic, and atmospheric contributions from the ECCO data assimilating ocean model, CPC hydrology, and NCEP reanalysis. We denote time series of the sum of these three effects (air + ocean + water) as AOW. A large part of the decadal variations in LOD are presumed to arise from exchange of angular momentum between mantle and core (Hide et al. 1993; Chao and Gross 1987). In the present study, we focus on contributions of air and water at an interannual time sfcale, so it is appropriate to remove these. We apply a Butterworth low-pass filter (see the MATLAB Help Manual) with a cutoff period of 8 years to estimate these very-low-frequency signals (see the green curve on Fig. 1c) and remove them from ΔC_{20}. The means over the 22-year period are removed from all time series, i.e. the time-variables ΔC_{21}, ΔS_{21}, and ΔC_{20} are relative to the 22-year means.

We remove seasonal and shorter period signals by smoothing with a 1-year sliding window. The resulting variations in ΔC_{21}, ΔS_{21}, and ΔC_{20} are shown in Fig. 2a,b,c. SLR estimates of ΔC_{20} variations, with the same smoothing, also appear in Fig. 2c. It is clear from Fig. 2a,b that ΔC_{21} and ΔS_{21} EOP and AOW time series agree remarkably well during the 22 year period. Figure 2c shows that EOP-derived ΔC_{20} variations are dominated by a strong oscillation with a period near 5.6 years, estimated through spectral analysis (Fig. 3). This is consistent with the findings of Abarca del Rio et al. (2000). Both SLR and AOW ΔC_{20} series show similar behavior, though with much smaller amplitudes. SLR and AOW ΔC_{20} time series agree reasonably well during most of the 22-year period, while differences increase following the 1997/1998 El Niño event, the start of the anomaly discovered by Cox and Chao (2002).

There appear some decadal scale variations in EOP-derived ΔC_{21} and ΔS_{21} time series, which are generally believed to be associated with contributions from core–mantle coupling (Hide et al. 1993). We apply the same low-pass filter with cutoff period of 8 years to estimate these decadal signals and remove them from EOP-derived ΔC_{21} and ΔS_{21} time series, and show the results and comparisons in Fig. 4a and b. We also remove the strong 5.6-years oscillation in EOP-derived ΔC_{20} series

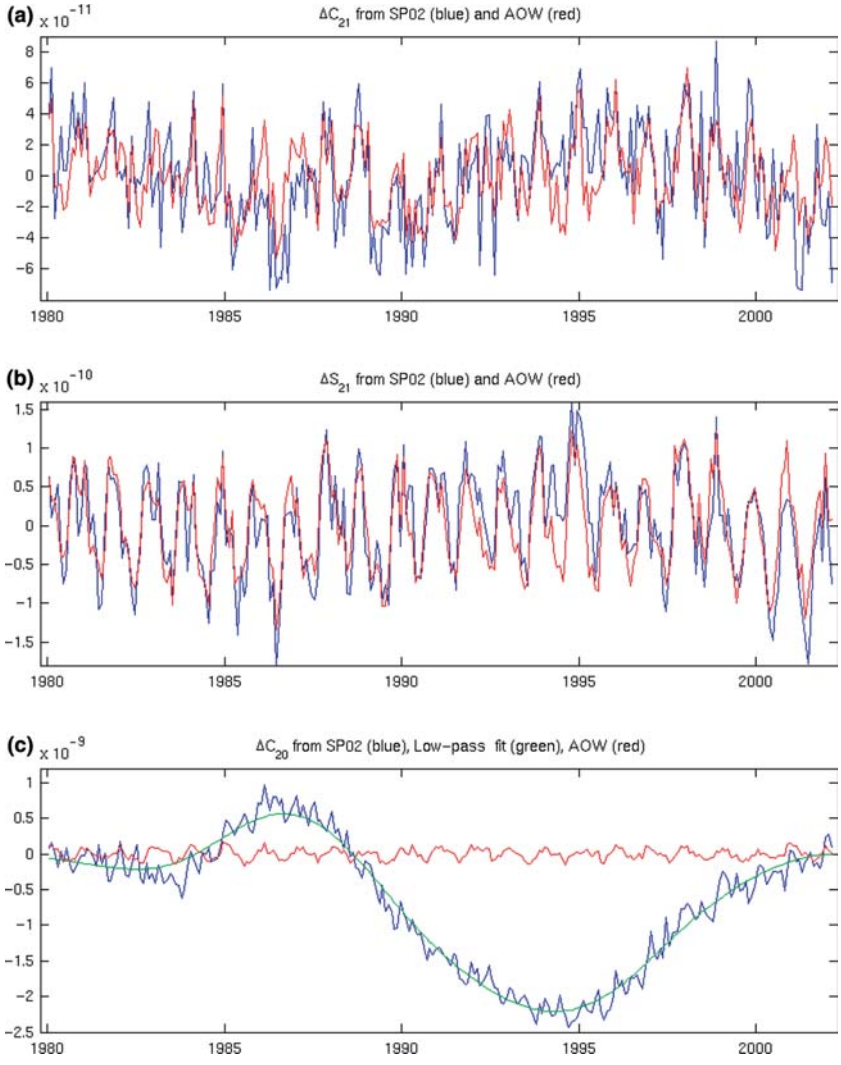

Fig. 1a,b,c. Estimated ΔC_{21}, ΔS_{21}, and ΔC_{20} variations from SP02 (*blue*) and geophysical models (AOW, *red*). The *green curve* in **c** shows the low-pass fit of LOD-derived ΔC_{20}

using a high-pass filter with a cutoff period of 5 years, and show the comparison in Fig. 4c. Apparently, the removal of decadal scale signals in EOP-derived ΔC_{21} and ΔS_{21} estimates significantly increases the agreement with model predictions, especially in ΔS_{21} estimates. With the 5.6-years oscillation removed, the residual EOP-derived ΔC_{20} results also show reasonable agreement with model predictions and SLR estimates. However, the agreement becomes worse during the 1982/1983 and 1997/1998 strong El Niño events. This can be attributed to the relatively larger uncertainties of geophysical models either in modeling mass redistribution during strong El Niño events that affect model predictions of these low-degree gravity changes, or in modeling winds and ocean currents which affect EOP-derived estimates.

We compute cross correlations between EOP-derived ΔC_{21}, ΔS_{21}, and ΔC_{20} time series and model predictions (as shown in Fig. 4). The results are shown in Fig. 5. This analysis further quantifies and demonstrates the good agreement between the two estimates. The maximum correlation coefficients at zero phase lag reach 0.56 and 0.68 for ΔC_{21} and ΔS_{21}, respectively, though there is no evident correlation peak (at zero phase lag) for ΔC_{20} estimates. Figure 6a,b,c show separate contributions from the atmosphere, ocean, and continental water. All three are important in interannual time series. However, we found that the atmosphere plays a relatively greater role in predicted ΔC_{20} change and continental water storage change appears more important in ΔS_{21} change (Fig. 6). Interestingly, the atmospheric contribution to ΔC_{20} seems to show a similar 5-year oscillation to that we found in the EOP-derived ΔC_{20} estimate, but its magnitude is too small to explain the EOP-derived estimate.

5 Discussion

Differences between the EOP and AOW ΔC_{21}, ΔS_{21}, and ΔC_{20} series shown in Fig. 2 are far greater than the errors associated with the EOP data. Based on the polar motion transfer function (Wilson 1985), at interannual and longer time scales, uncertainties of observed X_p, Y_p

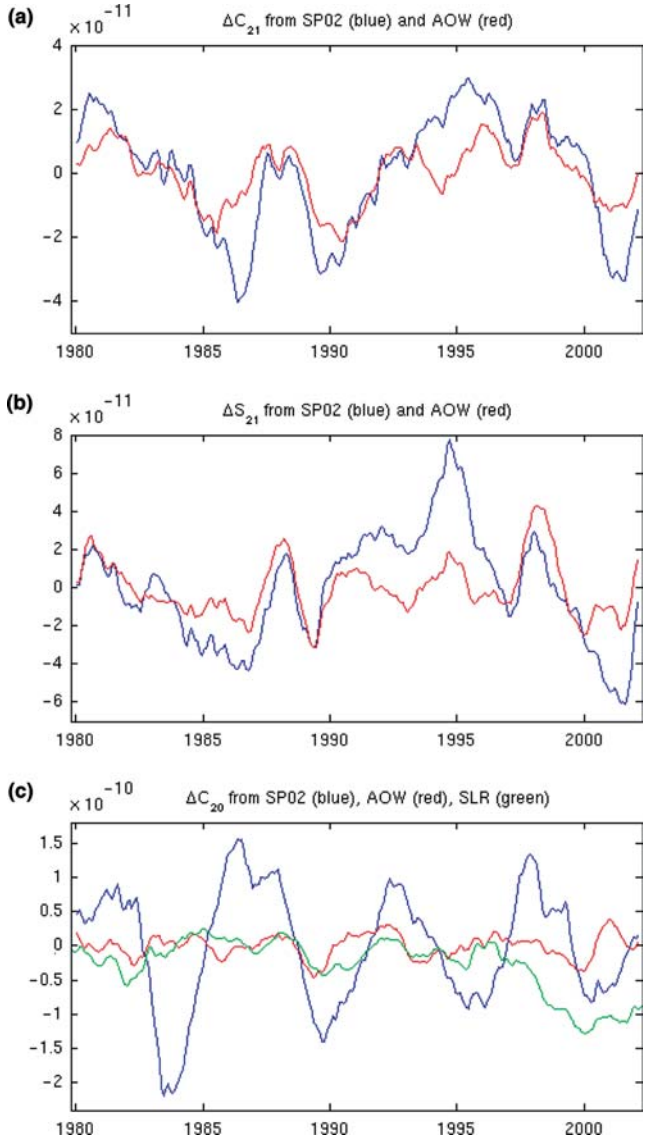

Fig. 2a,b,c. Interannual ΔC_{21}, ΔS_{21}, and ΔC_{20} variations from SP02 (*blue curves*) and geophysical model predictions (*red curves*). The *green curve* in **c** shows SLR-measured interannual ΔC_{20} variations

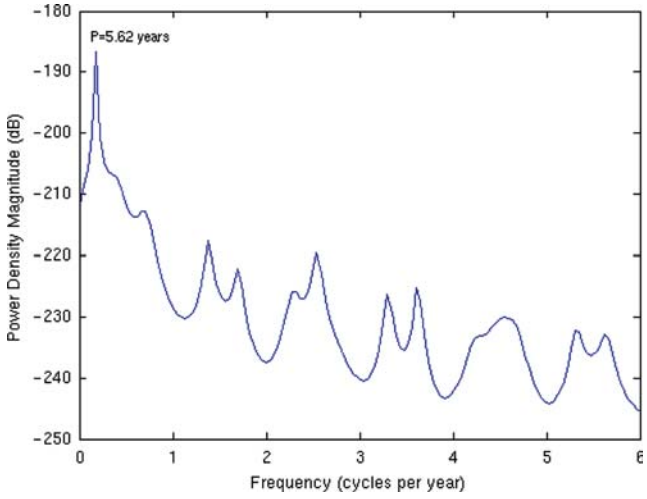

Fig. 3. Power spectrum density of EOP-derived ΔC_{20} variations as shown in Fig. 2c. The largest peak represents a period of 5.62 years. Decadal and longer periods are removed before the power spectrum analysis

time series are scaled to errors in excitations by a factor of less than 1. This means that we may take uncertainties of observed polar motion X, Y (below 0.1 mas in the late 1990s) as an upper bound on the errors of EOP-derived excitation time-series values. These scale to about 2×10^{-13} in terms of changes in the Stokes coefficients, which are less than 1% of the time-variable signals in the very low degrees. Therefore, differences in Fig. 2 must be associated with errors in hydrologic, oceanic, and atmospheric model estimates. These could be introduced in two ways: either in the wind and ocean current estimates that must be removed from the EOP series, or in the mass redistribution effects used to compute the AOW series.

The strong 5.6-year oscillation in EOP-derived ΔC_{20} variations is probably caused by errors in atmospheric winds, although Abarca del Rio et al. (2000) suggest that core–mantle interaction is the likely cause. The results from this study suggest that there is a near 5.6-year oscillation in the atmospheric general circulation system, which is not appropriately modeled (by NCEP reanalysis). This oscillation also affects atmospheric surface pressure change and therefore causes similar but much smaller changes in SLR and AOW ΔC_{20} time series (see Figs. 2 and 6). This study clearly demonstrates that accurately measured Earth rotational variations are an important and unique data resource to help to diagnose and constrain global-scale redistribution and movement in atmospheric and oceanic models.

An encouraging discovery is that, at interannual time scales, the current generation of oceanic, hydrologic, and atmospheric models do a good job of tracking mass redistribution within their separate elements of the climate. This bodes well for the ability of future coupled climate models to predict gravity field variations in a fully consistent way. A related conclusion is that climate models, even the current models that are not fully coupled, ought to be useful in validating time-variable gravity estimates provided by the Gravity Recovery and Climate Experiment (GRACE) and future gravity satellite missions. EOP data provide useful constraints on low-degree gravity variations at all time scales, and because they are available at high temporal sampling rates, EOP data should be useful in understanding the space–time aliasing expected in GRACE and other satellite gravity time–series. A recent paper by Reigber et al. (2003) demonstrates that the observations from the Challenging Minisatellite Payload for Geophysical Research (CHAMP) mission show a higher level of accuracy of the degree-two Stokes coefficients' change from CHAMP in comparison to traditional SLR determinations. Decadal time scale variations due to air and water appear in all three degree-two components of the gravity field examined here, and have the possibility of contaminating estimates of long-time-scale contribu-

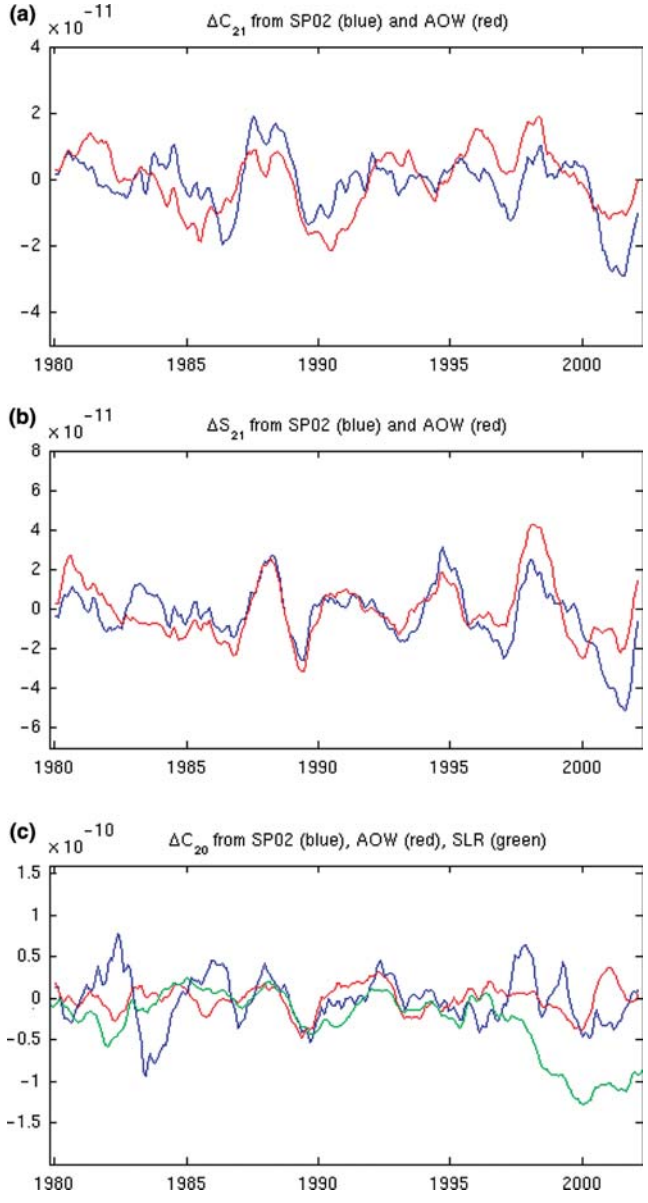

Fig. 4a,b,c. Interannual ΔC_{21}, ΔS_{21}, and ΔC_{20} variations from SP02 (*blue curves*) and geophysical model predictions (*red curves*). Decadal and longer periods are removed from EOP-derived ΔC_{21} and ΔS_{21} time series. The 5.6-year oscillation is also removed using a high-pass filter with a 5-year cutoff period. The *green curve* in **c** shows SLR–measured interannual ΔC_{20} variations

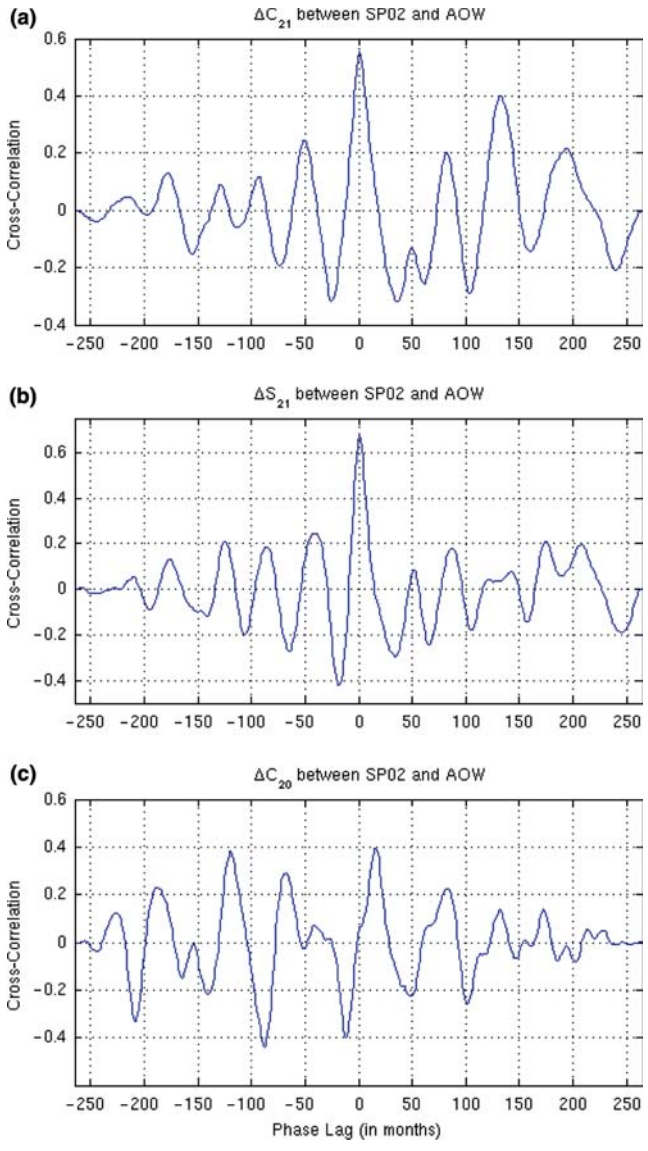

Fig. 5a,b,c. Cross-correlations between EOP-derived interannual ΔC_{21}, ΔS_{21}, and ΔC_{20} variations and model predictions (as shown in Fig. 4)

tions from other sources such as postglacial rebound or the core, given only the few decades of space geodetic observations now available.

6 Conclusion

Both EOP-derived results and model estimates show strong interannual variations in the degree-two gravitational change ΔC_{21}, ΔS_{21}, and ΔC_{20}. There is remarkably good agreement between EOP-derived and estimates from advanced atmospheric, oceanic, and hydrological models, in particular in ΔC_{21} and ΔS_{21}. Because of the dominant atmospheric wind effects on LOD change, EOP-derived ΔC_{20} is highly sensitive to uncertainties in atmospheric wind estimates, and therefore shows less agreement with model estimates. There is a strong 5.6-year oscillation in LOD excitations not accounted for by atmospheric and oceanic contributions estimated from the NCEP reanalysis and ECCO ocean general circulation models. After this 5.6-year oscillation, which is likely to be caused by atmospheric wind errors and/or core–mantle interaction, is removed from the LOD residuals, the LOD-derived ΔC_{20} also agrees reasonably well with SLR observations and model predictions at an interannual time scale during most of the 22-year period, with the exception of the strong 1982/1983 and 1997/1998 El Niño events.

Acknowledgments. The authors would like to thank R. Gross, A. Marchenko, an anonymous reviewer, and the editor-in-chief for

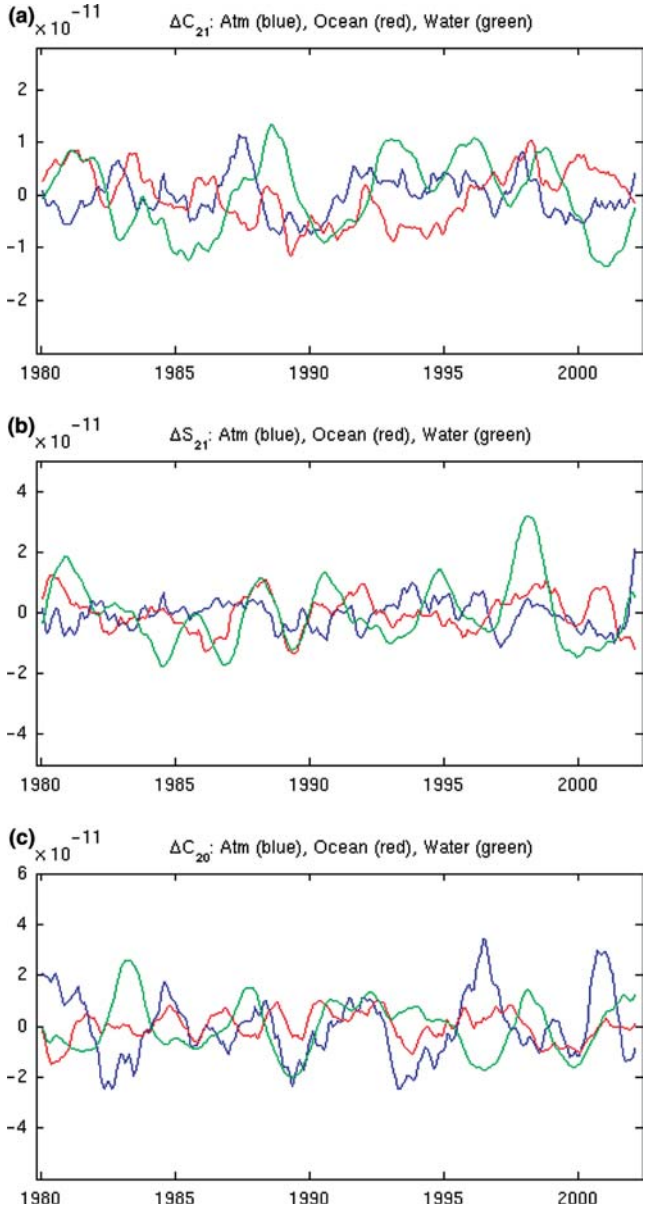

Fig. 6a,b,c. Atmospheric, oceanic and water contributions to interannual ΔC_{21}, ΔS_{21}, and ΔC_{20} variations

their insightful comments which led to improvements in the presentation and discussion of these results. They are grateful to Chris Cox for providing the satellite laser ranging data. This research was supported by NASA's Solid Earth and Natural Hazards and GRACE Program.

References

Abarca del Rio R, Gambis D, Salstein DA (2000) Interannual signals in length of day and atmospheric angular momentum. Ann Geophys 18(3):347–364

Barnes R, Hide R, White A, Wilson C (1983) Atmospheric angular momentum functions, length-of-day changes and polar motion. Proc R Soc Lond A387:31–73

Chao BF (1993) Geoid and its geophysical interpretation. In: Vanicek P Christou, NT (eds). CRC Press, Boca Raton, FL, pp 285–298

Chao BF, Au AY (1991) Atmospheric excitation of the Earth's annual wobble: 1980–1988. J Geophy Res 96:6577–6582

Chao BF, Eanes RJ (1995) Global gravitational changes due to atmospheric mass redistribution as observed by the Lageos nodal residual. Geophys J Int 122:755–764

Chao BF, Gross RS (1987) Changes in the Earth's rotation and low-degree gravitational field induced by earthquakes. Geophys J R Astron Soc 91:569–596

Chao BF, O'Connor WP (1988) Effect of a uniform sea-level change on the Earth's rotation and gravitational field. Geophys J R Astron Soc 93:191–193

Chao BF, Cox CM, Au A, Boy J (2003) Time-variable gravity from satellite-laser-ranging: low-degree components and geophysical/climatic connections. IUGG 2003 General Assembly, Sapporo, 30 June–11 July

Chen JL, Wilson CR (2003) Low degree gravitational changes from Earth rotation and geophysical models. Geophy Res Lett 30(24):2257–2260

Chen JL, Wilson CR, Eanes RJ, Tapley BD (1999) Geophysical contributations to satellite nodal residual variation. J Geophys Res 104(B10):23 237–23 244

Chen JL, Wilson CR, Eanes RJ, Tapley BD (2000) A new assessment of long wavelength gravitational variations. J Geophys Res 105(B7):16 271–16 278

Chen JL, Wilson CR, Hu XG, Tapley BD (2003) Large-scale mass redistribution in the oceans, 1993–2001, Geophys Res Lett 30(20):2024–2027

Cheng MK, Tapley BD (1999) Seasonal variations in low degree zonal harmonics of the Earth's gravity field from satellite laser ranging observations. J Geophys Res 104(B2):2667–2682

Cheng MK, Shum CK, Tapley BD (1997) Determination of long-term changes in the Earth's gravity field from satellite laser ranging observations. J Geophys Res 102:22 377–22 390

Cox CM, Chao BF (2002) Detection of a large-scale mass redistribution in the terrestrial system since 1998. Science 297: 831–833

Dickey JO, Marcus SL, Johns CM, Hide R, Thompson SR (1993) The oceanic contribution to the Earth's seasonal angular momentum budget. Geophys Res Lett 20(24):2953–2956

Dickey JO, Marcus SL, Olivier de Viron, Fukumori I (2002) Recent Earth oblateness variations: unraveling climate and post-glacial rebound effects. Science 298:1975–1977

Eubanks TM (1993) Variations in the orientation of the Earth. In: Smith D, Turcotte D (eds) Contributions of space geodesy to geodynamic: Earth dynamics, Geodyn Ser vol 24. AGU, Washington, DC, pp 1–54

Fan Y, Huug Van del Dool, Mitchell K, D. Lohmann D (2003) A 51-year reanalysis of the US land-surface hydrology. GEWEX News 13(2):6–10

Farrel WE (1972) Deformation of the Earth by surface loads. Rev Geophys Space Phys 10:761

Fukumori I, Lee T, Menemenlis D, Fu LL, Cheng B, Tang B, Xing Z, Giering R (2000) A dual assimilation system for satellite altimetry. Joint TOPEX/POSEIDON and Jason-1 Science Working Team Meeting, Miami Beach, FL, 15–17 November

Gross RS (2002) Combinations of Earth orientation measurements, SPACE2001, COMB2001, and POLE2001. Pub 02–08, Jet Propulsion Laboratory, Pasadena, CA

Gross RS, Fukumori I, Menemenlis D (2003) Atmospheric and oceanic excitation of the Earth's wobbles during 1980–2000. J Geophys Res 108 (B8):2370

Gross RS, Blewitt G, Clarke PJ, Lavallee D (2004a) Degree-2 harmonics of the Earth's mass load estimated from GPS and Earth rotation data. Geophy Res Lett 31:L07601

Gross RS, Fukumori I, Menemenlis D, Gegout P (2004b) Atmospheric and oceanic excitation of length-of-day variations during 1980–2000. J Geophys Res 109(B1):B01406

Hide R, Clayton RW, Hager BH, Spieth MA, Voorhies CV (1993) Topographic core–mantle coupling and fluctuations in the Earth's rotation. In: Dmawska R (ed) Relating geophysical structures and processes. The Jeffreys volume, Geophys Monogr Ser No. 76. AGU, Washington, DC, pp 107–120

Kantha LH, Stewart JS, Desai SD (1998) Long-period lunar fortnightly and monthly ocean tides, J Geophys Res 103:12 639–12 647
Lambeck K (1980) The Earth's variable rotation. Cambridge University Press, Cambridge
Marchenko AN, Schwintzer P (2003) Estimation of the Earth's tensor of inertia from recent global gravity field solutions. J Geod 76(9–10):495–509
Nerem RS, Eanes RJ, Thompson P, Chen JL (2000) Observations of annual variations of the Earth's gravitational field using satellite laser ranging and geophysical models. Geophy Res Lett 27 (12):1783–1786
Nerem RS, Leuliette EW, Parker JS, Gross RS, Cazenave A, Lemoine JM, Chambers DP (2002) An investigation of recent observed changes in the Earth's oblateness. AGU 2002 Fall Meeting, San Francisco, 6–10 December
Pavlis E (2001) Dynamical determination of origin and scale in the Earth system from satellite laser ranging. In: Adam J Schwarz K-P (eds) Vistas for geodesy in the new millennium. IAG Symp vol 125. Springer, Berlin Heidelberg New York, pp 36–41
Ponte RM, Stammer D, Marshall J (1998) Oceanic signals in observed motions of the Earth's pole of rotation. Nature 391:476–479
Reigber Ch, Jochmann H, Wünsch J, Neumayer KH, Schwintzer P (2003) First insight into temporal gravity variability from CHAMP. In: Reigber Ch, Lühr H, Schwintzer P (eds) "First CHAMP mission results for gravity, magnetic and atmospheric studies. Springer; Berlin Heidelberg, New York, pp 128–133
Rochester M, Smylie D (1974) On changes in the trace of the Earth's inertia tensor. J Geophys Res 79(2):4948–4951
Rubincam DP (1984) Postglacial rebound observed by Lageos and the effective viscosity of the lower mantle. J Geophys Res 89:1077–1087
Salstein DA, Rosen RD (1997) Global momentum and energy signals from reanalysis systems. Preprints, 7th Conf, on Climate Variations. American Meteorological Society, Boston, MA, pp 344–348
Stephenson FR, Morrison LV (1995) Long-term fluctuations in Earth's rotation 700BC to AD 1990. Phil Trans Phys Sci and Engng, 351(1695):165–202
Wilson CR (1985) Discrete polar motion equations. Geophys J R Astron Soc 80:551–554
Yoder CF, Williams JG, Parke ME (1981) Tidal variations of Earth rotation. J Geophys Res 86:881–891
Yoder CF, Williams JG, Dickey JO, Schutz BE, Eanes RJ, Tapley BD (1983) Secular variation of Earth's gravitational harmonic J coefficient from Lageos and non-tidal acceleration of Earth rotation. Nature 303:757–762